A Novel Trench-Assisted Optical Fiber With Ultra-Low Microbending Loss for the Full Ocean Depth Communication

Ruipu Li, Chuanlu Deng, Yi Huang, *Member, IEEE*, Zhenyi Chen, Xiaobei Zhang, and Tingyun Wang, *Member, IEEE*

***Abstract*—A novel trench-assisted optical fiber with ultra-low microbending loss is proposed, which contains two trenches beside the core. The deformation distribution of the fiber axis caused by the wire mesh is in agreement with a Gaussian curve through the mechanical-optical model. By analyzing the microbending loss dependency on the optical fiber parameters, the optimal structure for the trench-assisted optical fiber was obtained. The fundamental mode field characteristics of the designed fiber under microbending were simulated using the finite element method, and the energy ratio of the designed fiber was obtained as 95.03%, which is larger than that of the conventional single-mode fiber. The designed fiber was fabricated based on the modified chemical vapor deposition (MCVD) technique and tested according to the modified plate method. The experimental results indicate that the fabricated fiber can support an ultra-low microbending loss of 0.0052 dB/m at 6 kg weight at 1550 nm, which is reduced by two orders of magnitude compared to the conventional single-mode fiber. The microbending loss measurement system exhibits good reliability and repeatability, and the measured results are consistent with the theory. The proposed optical fiber will be beneficial in improving the transmission efficiency of full ocean depth communication.**

***Index Terms*—Full ocean depth communication, microbending loss, microbending-resistant fiber, trench-assisted profile.**

I. Introduction

THE fiber optic micro-cable (FOMC) is widely used in deep-ocean exploration to establish a reliable communication channel between the underwater vehicle and the mother ship [1]. For example, the "Nereus" hybrid remotely operated vehicle (HROV) in the United States successfully dived into the hadal ocean depth of 10903 m of the Mariana Trench using the FOMC as a communication medium [2]. The FOMC generally consists of optical fiber, reinforcement layer, and outer sheath, with a diameter of about 1 mm [3]. In the complex deep-ocean environment, the additional attenuation caused by the lateral water pressure mainly comes from microbending attenuation [4]. Under high water pressure, the slight irregularities on the inner surface of the reinforcement layer lead to uneven stress of each part of the optical fiber, resulting in random microbendings [5]. In this case, the transmission loss of the conventional single-mode optical fiber will increase. When the loss exceeds a certain threshold, the signal transmission will be terminated [4]. Therefore, improving the microbending performance of optical fibers is the key to achieving effective data transmission in deep-ocean exploration.

The theoretical research on microbending-induced loss in the conventional single-mode and multimode fiber has been gradually developed. In 1975, R. Olshansky et al. analyzed the distortion loss caused by imperfections in the cable using a simple cable model [6]. In 1976, K. Petermann et al. introduced a quasi-mode that approximates the true field distribution of all cladding modes for calculating the coupling losses due to microbendings [7]. In 1984, D. Marcuse et al. further took the coupling losses caused by microbendings along the fiber axis and random fluctuations of the core diameter into account [8]. However, most of the previous analysis on microbending loss was based on assumed microbending deformation distribution [6], [7], [8]. In 2022, Z. Várallyay et al. found that the deformation function of the fiber axis caused by sandpaper particles resembles a Gaussian curve through a mechanical model [9]. However, this mechanical model only demonstrates the mechanical properties of the optical fiber without the optical properties. In addition, the wire mesh is also commonly used to induce microbending, but there are few investigations on the mechanism of microbending caused by the wire mesh.

The microbending-resistant optical fibers have been attracting growing attention in reducing the additional attenuation of the FOMC in the deep ocean. There are two approaches to reducing the microbending sensitivity of optical fiber. One is to optimize the optical fiber structure, the other is to use a dual-coating system with a softer primary coating [10]. In earlier research, holey, microstructured, and trench-assisted optical fibers were found to exhibit excellent resistance to microbending. Nonetheless, it is difficult to achieve good transmission loss properties and mass production for holey and microstructured optical fibers [11], [12]. Trench-assisted optical fibers can overcome the drawbacks

Manuscript received 28 April 2023; revised 15 August 2023; accepted 22 September 2023. Date of publication 29 September 2023; date of current version 25 October 2023. This work was supported by the National Natural Science Foundation of China under Grants 61735009 and 62027818. *(Corresponding author: Tingyun Wang.)*

The authors are with the Key Laboratory of Specialty Fiber Optics and Optical Access Networks, Joint International Research Laboratory of Specialty Fiber Optics and Advanced Communication, Shanghai Institute for Advanced Communication and Data Science, Shanghai University, Shanghai 200444, China (e-mail: ruipuli@shu.edu.cn; chuanludeng@163.com; huangyi1008@shu.edu.cn; zychen@shu.edu.cn; xbzhang@shu.edu.cn; tywang@shu.edu.cn).

Digital Object Identifier 10.1109/JPHOT.2023.3319493

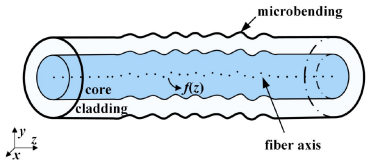

Fig. 1. Random bends in an optical fiber.

of the above two types of fibers [13], [14], [15], [16], [17]. The single-trench-assisted fiber can reach lower microbending losses with weaker wavelength dependence compared to the conventional single-mode fibers [10]. An optimized single-trench-assisted optical fiber can achieve a low microbending loss of 14.7 dB/km at 1550 nm [18]. In [4], a new optical fiber structure with a deep trench beside the inner cladding was investigated. However, the refractive index difference of the trench is −0.67%, which approaches a limit value of −0.7% achievable for the fluorine doping process [19]. Furthermore, placing the trench beside the core is the key to achieving ultra-low bending loss by comparing the four-cladding structure with the trench beside the core and the five-cladding structure with the trench beside the inner cladding [20]. The optical fiber structure with the trench beside the core may also have a positive impact on the microbending loss, but there is little research on this aspect. Therefore, it is necessary to investigate the effect of this structure on the microbending performance.

In this study, a trench-assisted microbending-resistant optical fiber is proposed, which features two trenches beside the core, with the refractive index of the inner trench lower than that of the outer trench. Firstly, a mechanical-optical model was constructed to obtain the deformation distribution of the fiber axis caused by the wire mesh, and the formula for the microbending loss was derived. Furthermore, the optimum structure of the trench-assisted optical fiber was obtained through a simulation of the microbending loss based on the coupled mode theory. The fundamental mode field properties and the core energy ratio of the designed fiber were discussed in detail, compared with commercially available conventional single-mode fiber (SMF-28e), three types of bending-resistant single-mode fibers (G.657A1, G.657A2, G.657B3). Subsequently, the designed fiber was fabricated based on the MCVD technique, and the structure size and the refractive index profile of the fabricated fiber were measured using an optical fiber analyzer. Finally, an experimental setup for the microbending loss measurement was established. The microbending loss characteristics of the fabricated fiber were investigated both theoretically and experimentally.

II. Microbending Theory

For an ideal optical fiber, the fiber axis is perfectly straight. However, the fiber axis randomly deviates from the ideal straight line [21] under high water pressure in the complex deep-ocean environment. The deviation from the ideal straightness of an optical fiber can be expressed as random bends, also called microbending [22], as demonstrated in Fig. 1. Such deviation can be described by the deformation distribution $f(z)$ of the fiber axis [7]. The microbending loss occurs due to the coupling between the fundamental guided mode and the radiation modes [10].

In Petermann's theory [22], the microbending loss α can be defined as

$$\alpha = \frac{1}{4}(kn_1w_0)^2\Phi(\Delta\beta), \tag{1}$$

with

$$\Delta\beta = \beta_0 - \beta_p = 1/(kn_1w_0^2), \tag{2}$$

$$w_0^2 = \frac{\int_0^\infty r^3E_0(r)^2dr}{\int_0^\infty rE_0(r)^2dr}, \tag{3}$$

where k is the free space wave number, n_1 is the core refractive index, w_0 is the normalized spot radius, $\Phi(\Delta\beta)$ is the power spectrum of the axis curvature, $\Delta\beta$ is the propagation constant difference between the fundamental mode propagation constant β_0 and the "quasi-mode" propagation constant β_p, r is the normalized radial coordinate, and $E_0(r)$ is the transverse fundamental mode field. The power spectrum $\Phi(\Delta\beta)$ of the deformation distribution $f(z)$ is given by

$$\Phi(\Delta\beta) = \lim_{L\to\infty}\frac{1}{L}\int_0^L\left|f''(z)e^{-j\Delta\beta z}dz\right|^2, \tag{4}$$

where L is the length of the deformation and z is the axial coordinate. The power spectrum is generally assumed to be of the form $1/\Delta\beta^{2p}$ introduced by Petermann [22] with $p = 0$, 1, 2. The parameter p is an additional exponential factor that determines the statistical character of curvature.

The microbending loss measurement was performed using the modified plate method [23] based on IEC-TR62221 Method C [24]. To investigate the fiber deformation induced by the wire mesh, a mechanical-optical model was established using the finite element software COMSOL Multiphysics, as depicted in Fig. 2(a). The model contains a section of fiber, a piece of wire mesh with a mesh number of 20, a base plate, and a top plate. The optical fiber is placed in the middle of the base plate, with the wire mesh and the top plate placed above it. Three constraints are defined for the model in COMSOL software. The first one is that the end facets of the optical fiber are not allowed to move in the x and z directions, only up and down in the y direction. The second one is to apply a fixed constraint on the base plate to limit its movement. The third one is to set the top plate as a "rigid body". The top plate is only used to simulate the pressing process, so its deformation can be neglected. After completing these basic settings of the model, the pressure is applied to the top plate with a magnitude comparable to the weight used in the experiment. In addition, a 1 W light signal with a wavelength of 1550 nm is fed into the optical fiber.

The stress distribution of the optical fiber at 6 kg weight is obtained by simulation, as illustrated in Fig. 2(b). On the surface of the optical fiber, four distinct stress concentrations (U_1, U_2, U_3, and U_4) can be observed, and the stress distribution on the upper and lower surfaces is symmetrical. At the stress concentrations, the refractive index profile of the optical fiber changes due to the compressive stress. The total internal reflection condition of light is affected greatly, resulting in light leakage from the optical

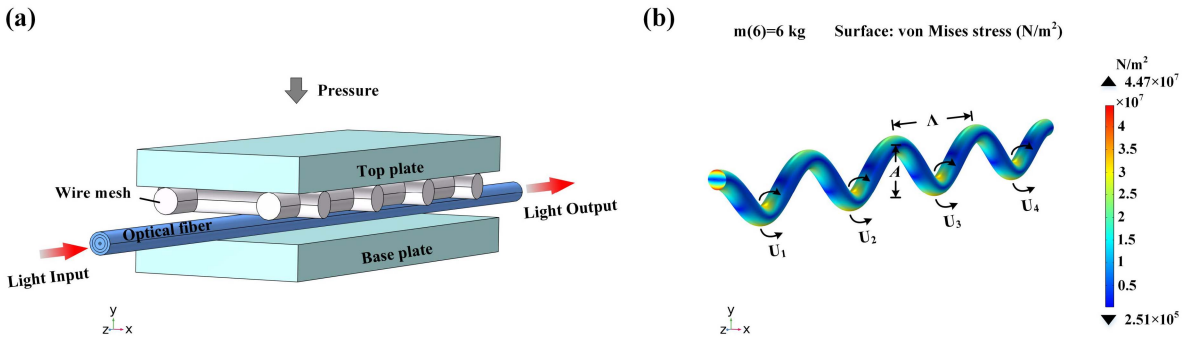

Fig. 2. (a) Mechanical-optical model to calculate the deformation of a section of fiber, including primary and secondary coatings; (b) stress distribution of the optical fiber at 6 kg weight in the contact area of the optical fiber and the wire mesh, and the deformation of the optical fiber magnified by 300 times.

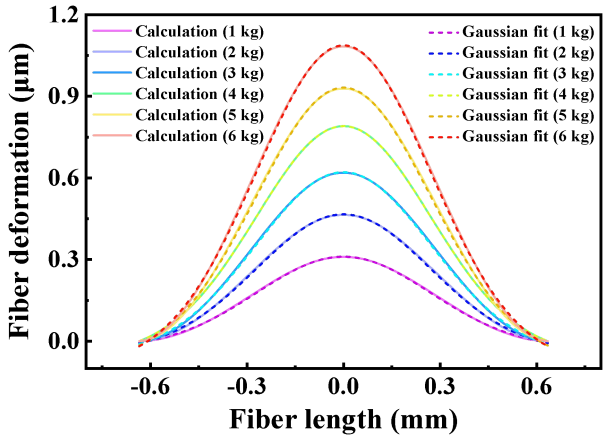

Fig. 3. Deformation function of the fiber axis along with the fitted Gaussian function at weights ranging from 1 kg to 6 kg.

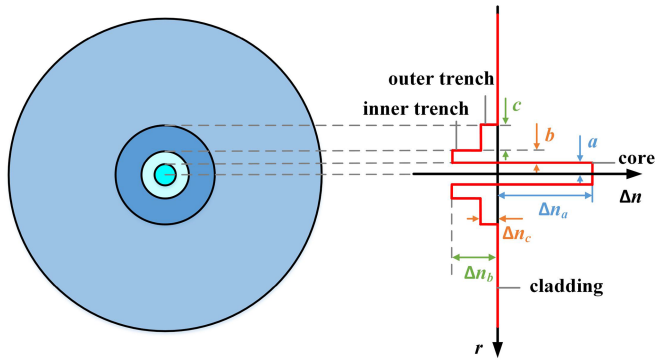

Fig. 4. Cross-section and refractive index profile of the designed fiber.

fiber and originating microbending loss [25]. Furthermore, the deformation distribution of the optical fiber is periodic with the period $\Lambda = 1.27$ mm. Within one period, the deformation of the fiber axis is maximum at the point of stress concentration due to the force applied by the wire mesh. The deformation amplitude A is dependent on the diameter of the optical fiber and the thickness of the coating [9].

In order to further analyze the amplitude and shape of the fiber deformation at weights ranging from 1 kg to 6 kg, the deformation function of the fiber axis for one period centered on U_3 is intercepted, as depicted in Fig. 3. The deformation amplitude of the fiber axis increases with the weight. The mechanical-optical model considers the stiffness of the glass and the coating, using a standard glass diameter of 125 μm and a standard coating thickness of 250 μm outer diameter. The deformation amplitude of the fiber axis is on the order of micrometers, consistent with the recent experimental results using a multi-core fiber to determine the amplitude of microdeformations—approximately 1 μm or less [26]. Moreover, the deformation function of the fiber axis is found to be in good agreement with a Gaussian curve. The deformation function is expressed as a Gaussian function: $f(z) = A\cdot\exp(-z^2/(2B^2))$, where B is the standard deviation of the Gaussian function. Using (4), its power spectrum function can be obtained as follows

$$\Phi(\Delta\beta) = 2\pi A^2 B^2 \Delta\beta^{4p} e^{-B^2\Delta\beta^{2p}}. \tag{5}$$

After obtaining the power spectrum of the fiber deformation, the theoretical microbending loss can be calculated according to (1).

III. Design and Simulation

A. Design of the Optical Fiber

As mentioned in the introduction, the trench-assisted structure can effectively reduce the microbending loss of the optical fiber. In this case, the fundamental guided mode is mainly coupled to a leaky 1st-higher order mode, which is a Lorentzian superposition of radiation modes that are resonantly confined by the trench. But for the step-index fiber, the fundamental guided mode is coupled to the continuum of radiation modes, which leads to a large coupling loss [10].

The proposed trench-assisted optical fiber contains two trenches with low refractive index, in which the inner trench is beside the core and the outer trench is between the inner trench and the cladding. The cross-section and the refractive index profile of the designed fiber are depicted in Fig. 4. The parameters a, b, and c are the radius of the core, the width of the inner trench, and the width of the outer trench, respectively. The radius of the cladding is 62.5 μm. Δn_a, Δn_b, and Δn_c are

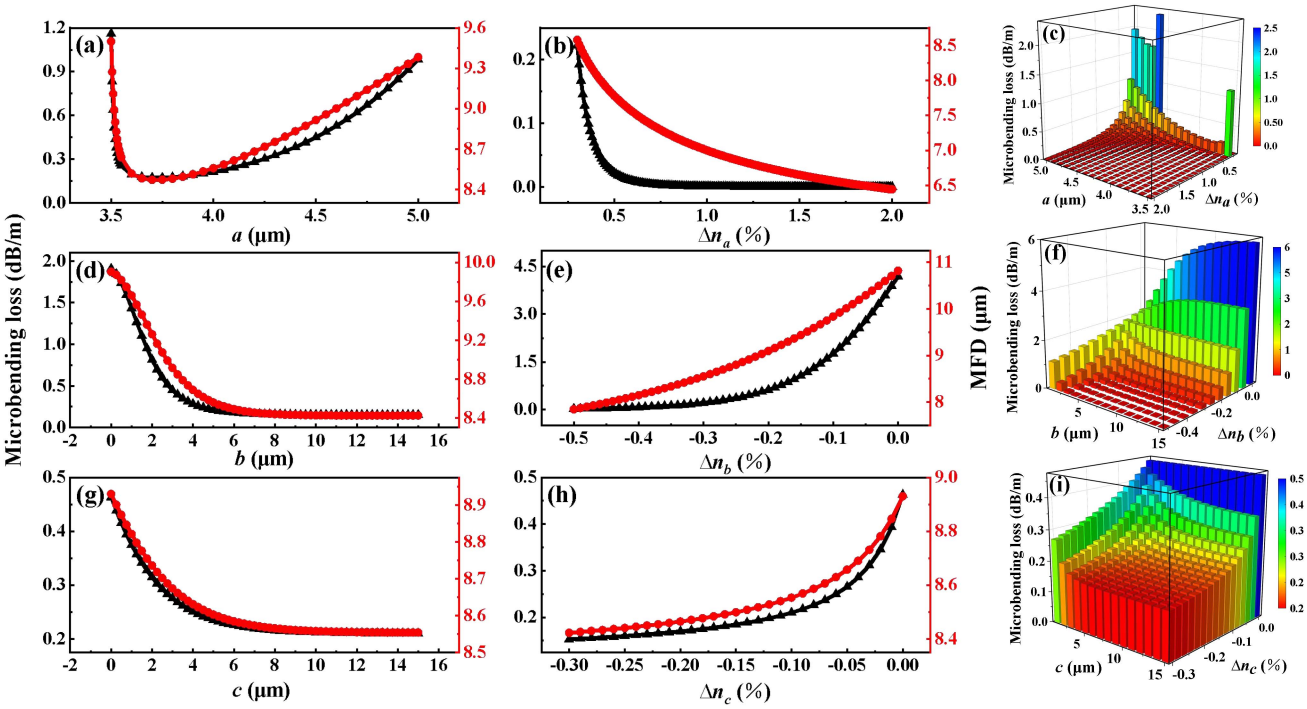

Fig. 5. Calculated dependences of the microbending loss and the mode field diameter on structural parameters at 6 kg weight at 1550 nm.

TABLE I
STRUCTURE PARAMETERS OF OPTICAL FIBERS

Fiber structure	Δn_a (%)	Δn_b (%)	Δn_c (%)	a (μm)	b (μm)	c (μm)
Initial fiber	0.3	-0.3	-0.1	4	5	10
Designed fiber	0.9	-0.5	-0.3	3.7	5	7

the relative refractive index differences between the core and the cladding, between the inner trench and the cladding, and between the outer trench and the cladding, respectively. In contrast to the traditional trench-assisted optical fibers, the designed fiber features two trenches beside the core, with the refractive index of the inner trench lower than that of the outer trench.

In the design, the initial fiber structural parameters are shown in Table I. The optimization rule is that one single structural parameter is varied over a reasonable range while the other structural parameters keep constant [16], in order to obtain a lower microbending loss. The effect of structural parameters on the microbending loss and the mode field diameter (MFD) at 6 kg weight at 1550 nm is presented in Fig. 5. It can be observed that the microbending loss and the MFD follow the same trend that its first decrease rapidly and then increase gradually with the increase of the core radius a, as shown in Fig. 5(a). The minimum microbending loss and the MFD both exist at the optimum value of $a = 3.7$ μm, which attributes to that the microbending loss essentially depends on the MFD of the optical fiber [7]. From Fig. 5(b), the microbending loss decreases rapidly and then gradually becomes flat and approaches zero with increasing Δn_a. The growth of Δn_a cannot infinitely improve the microbending performance of the optical fiber, and the value of Δn_a is finally chosen as 0.9%. For the inner trench, the microbending loss decreases with the width and depth of the inner trench, and eventually trends to a constant value, as demonstrated in Fig. 5(d) and (e). Considering the difficulty in fabrication and microbending performance, the inner trench width b and the refractive index difference Δn_b are determined to be 5 μm and -0.5%, respectively. An additional shallow outer trench is added to further reduce the microbending loss. In Fig. 5(g) and (h), the variation trend of the microbending loss with the width and the refractive index difference of the outer trench is similar to that of the inner trench. After comprehensive consideration, the optimized structural parameters of the designed fiber are determined and are listed in Table I. To further validate the rationality of the chosen combination of structural parameters, simulations were conducted on pairwise parameter combinations, as illustrated in Fig. 5(c), (f), and (i). It can be observed that the overall trend of the microbending loss is consistent with the left side of Fig. 5. Besides, the structural parameters of the designed fiber exist within a range where the microbending loss is sufficiently low.

B. Simulation Analysis

Generally, most of the light energy is confined to the core when the optical fiber is straight. However, the light energy is leaked from the core into the cladding and external environment at a sharp microbending [27]. The mechanical-optical model was employed to obtain the fundamental mode field distribution at the cross-section of the stress concentration U_3 (shown in Fig. 2(b)). The fundamental mode fields of SMF-28e, G.657A1, G.657A2, G.657B3 and the designed fiber at 6 kg weight at 1550

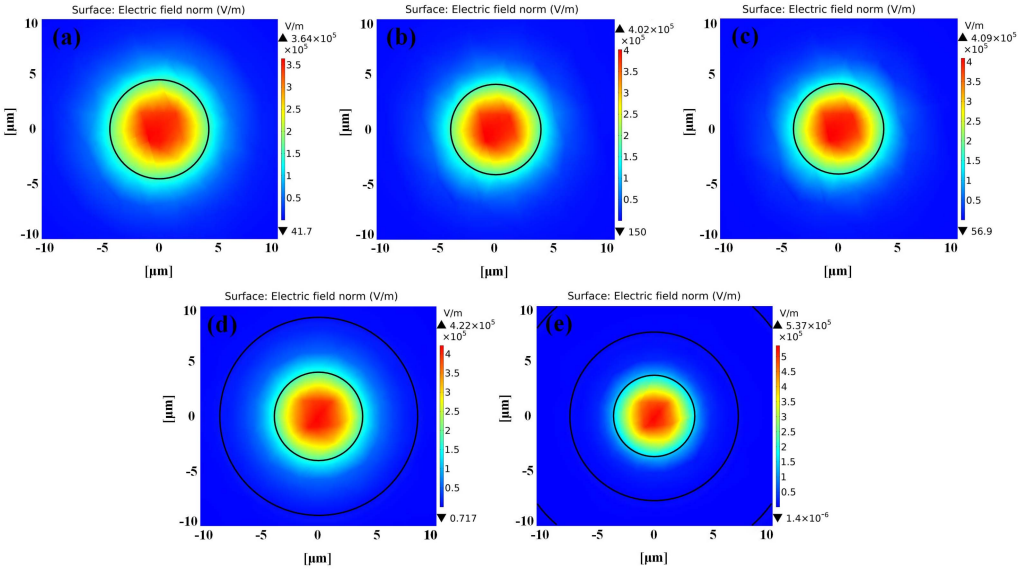

Fig. 6. Fundamental mode field distributions at 6 kg weight at 1550 nm. (a) SMF-28e, (b) G.657A1, (c) G.657A2, (d) G.657B3, (e) designed fiber.

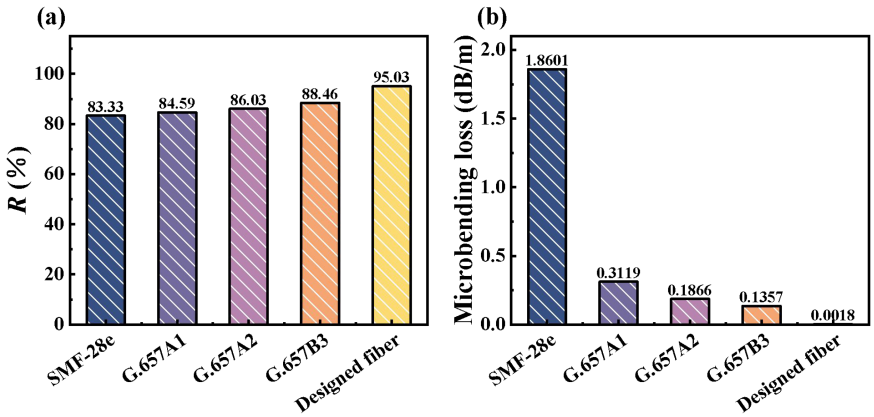

Fig. 7. (a) Core energy ratios and (b) the theoretical microbending losses of SMF-28e, G.657A1, G.657A2, G.657B3, and the designed fiber at 6 kg weight at 1550 nm.

nm are depicted in Fig. 6. The simulation results indicate that the five fibers exhibit varying degrees of light energy leakage from the core into the cladding. A significant light energy leakage can be observed from the mode field distribution of SMF-28e. Compared to SMF-28e, G.657A1, G.657A2, and G.657B3 all exhibit stronger light confinement capability due to their deeper trenches in the cladding. Among the five fibers, the designed fiber demonstrates the strongest light confinement capability. This is because the two trenches with low refractive index effectively prevent light energy leakage, allowing most of the energy to be confined in the core region.

The core energy ratio is an important parameter to measure the microbending loss characteristic of optical fibers. The core energy ratio R is denoted as $R = P_{\text{core}}/P_{\text{overall}}$, where P_{core} is the power in the core region, and P_{overall} is the power in the entire cross-section of the optical fiber [28]. P_{core} and P_{overall} can be calculated by the surface integral of the time-average power flow z-component [29] over the core region and the entire cross-section region of the optical fiber, respectively. The core energy ratios of the five fibers at the cross-section of the stress concentration U_3 are illustrated in Fig. 7(a). A significant difference between SMF-28e and the designed fiber can be observed in terms of the core energy ratios, which are 83.33% and 95.03%, respectively. In addition, the core energy ratios of G.657A1, G.657A2, and G.657B3 are 84.59%, 86.03%, and 88.46%, respectively. It is evident that the designed fiber can concentrate most of the energy in the core region under the same microbending conditions compared to the other four fibers. In addition, the theoretical microbending losses for the five fibers were obtained based on (1), as presented in Fig. 7(b). Theoretical results indicate that the microbending loss of the designed fiber is 0.0018 dB/m at 6 kg weight at 1550 nm. The microbending loss performance of the designed fiber has been significantly improved compared to the other four optical fibers. One possible

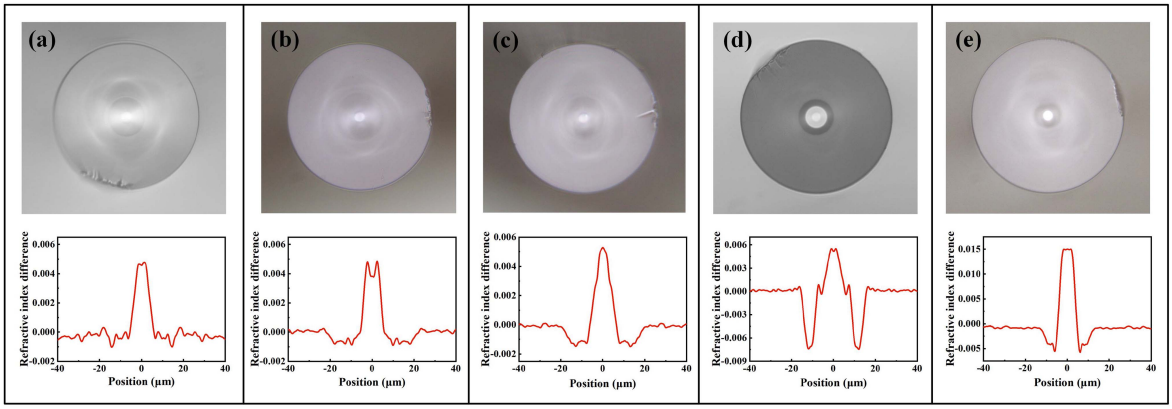

Fig. 8. Cross-section photographs under a microscope and refractive index profiles. (a) SMF-28e, (b) G.657A1, (c) G.657A2, (d) G.657B3, (e) fabricated fiber.

reason is that the field confinement effect of the trenches beside the core in the designed fiber structure has a positive effect on the microbending loss. Furthermore, the cutoff wavelength of the designed fiber is calculated to be 1480 nm, allowing the single-mode transmission at 1550 nm wavelength.

In practical fabrication, the structural parameters of the fiber cannot be accurately controlled arising from process nonuniformity or limitations in reproducibility [16]. It is extremely necessary to investigate the effect of process tolerances on microbending loss. The typical technical tolerances employed are as follows [30]: $a = \pm 1\%$, $b = \pm 1\%$, $c = \pm 1\%$, $\Delta n_a = \pm 2 \times 10^{-4}$, $\Delta n_b = \pm 2 \times 10^{-4}$, $\Delta n_c = \pm 2 \times 10^{-4}$. In the simulation, one single parameter is varied over a certain range while keeping the other parameters constant at 6 kg weight at 1550 nm. The parameters are fixed to the design values listed in Table I. For the structural parameters a, b, c, Δn_a, Δn_b and Δn_c, the changes of the microbending loss are 6.58×10^{-4} dB/m, 4.89×10^{-6} dB/m, 1.99×10^{-6} dB/m, 8.03×10^{-5} dB/m, 7.81×10^{-4} dB/m and 2.67×10^{-5} dB/m. These changes are sufficiently low for all technological tolerances separately. It indicates that the practical fabrication of the designed fiber exhibits reproducibility.

IV. Fabrication and Measurement

A. Fabrication of the Designed Fiber

The designed fiber was fabricated based on the MCVD technique. Germanium doping can increase the core refractive index, and fluorine doping can form the trench. Firstly, a high-purity fused silica tube with an outer diameter of 18 mm and a wall thickness of 1.2 mm was used as the substrate. Subsequently, the fluorine-doped trench was deposited with $SiCl_4$, O_2, and Freon as starting reactants. The germanium-doped core was then deposited with $SiCl_4$, O_2, and $GeCl_4$. The deposition process was carried out at approximately 1650 °C. After the deposition process, the supporting tube was collapsed into a preform at around 2000 °C. Finally, the preform was placed onto the drawing tower and drawn into an optical fiber at about 1850 °C. By using an optical fiber analyzer (NR9200, EXFO), the refractive index profile of the fabricated fiber was measured.

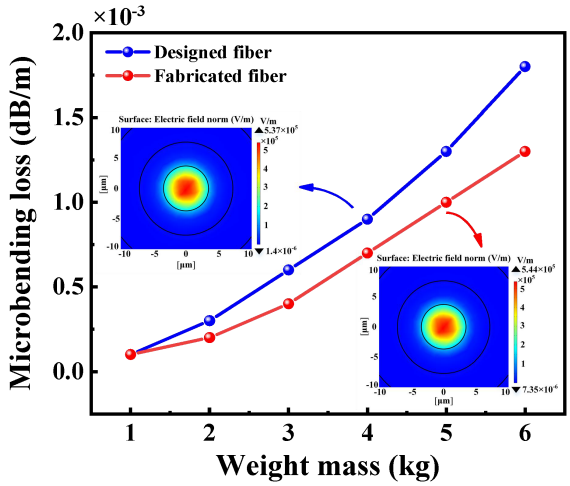

Fig. 9. Calculated microbending losses of the designed fiber and the fabricated fiber. The inset is the fundamental mode field distribution of the designed fiber and the fabricated fiber at 6 kg weight at 1550 nm.

TABLE II
Structural Parameters of Optical Fibers

Parameter	SMF-28e	G.657A1	G.657A2	G.657B3	Fabricated fiber
Δn_a (%)	0.42	0.47	0.51	0.55	1.47
Δn_b (%)	-0.007	-0.085	-0.12	-0.03	-0.45
Δn_c (%)	0	0	0	-0.68	-0.32
a (μm)	4.5	4.1	4.1	4.0	3.7
b (μm)	11.2	17.4	15.7	4.9	4.2
c (μm)	0	0	0	6.2	6.5

The cross-section photographs and refractive index profiles of SMF-28e, G.657A1, G.657A2, G.657B3, and the fabricated fiber are displayed in Fig. 8. The measured fiber structural parameters are shown in Table II. It is clear that the measured structural parameters of the fabricated fiber conform well to the design.

Furthermore, the microbending characteristics of both the designed fiber and the fabricated fiber are illustrated in Fig. 9. It can be observed that the microbending losses of the designed

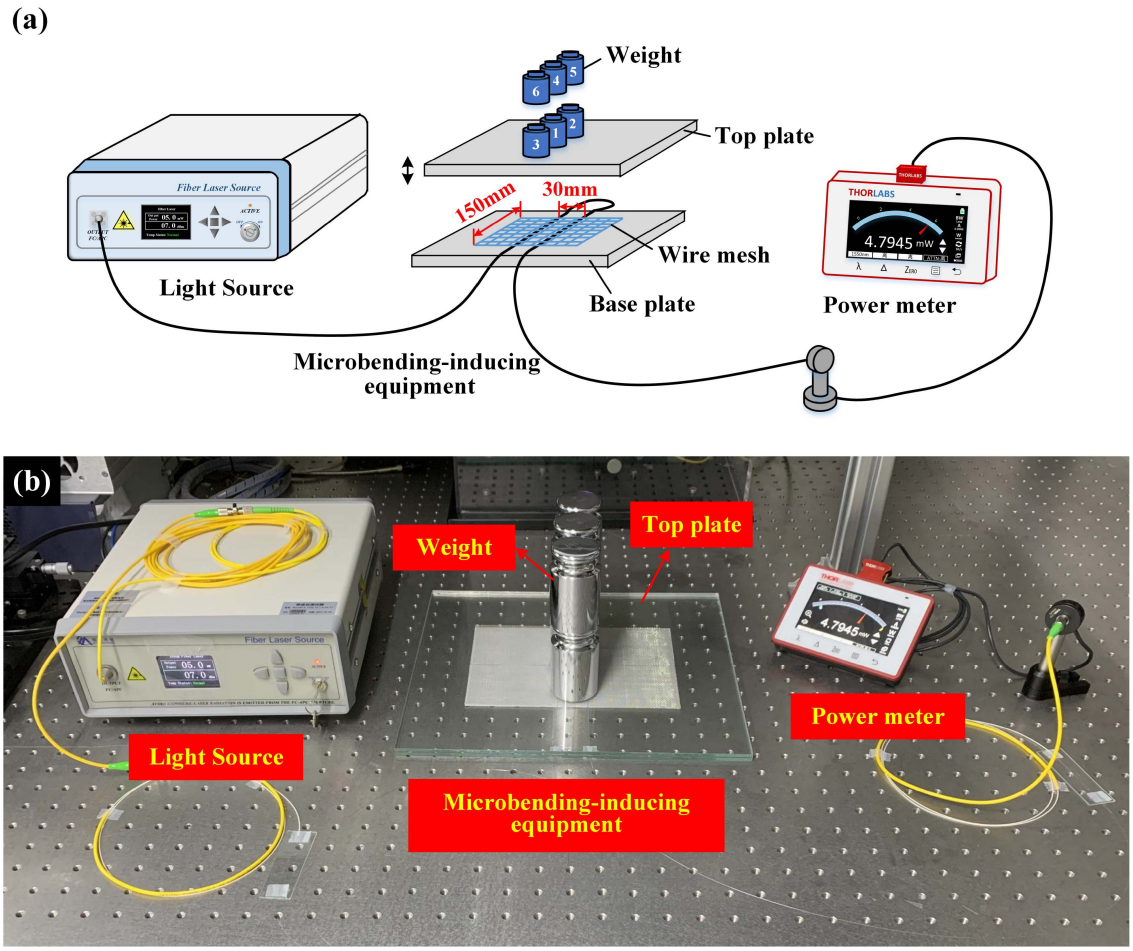

Fig. 10. (a) Microbending loss measurement system; (b) photograph of the experimental setup for the microbending loss measurement system.

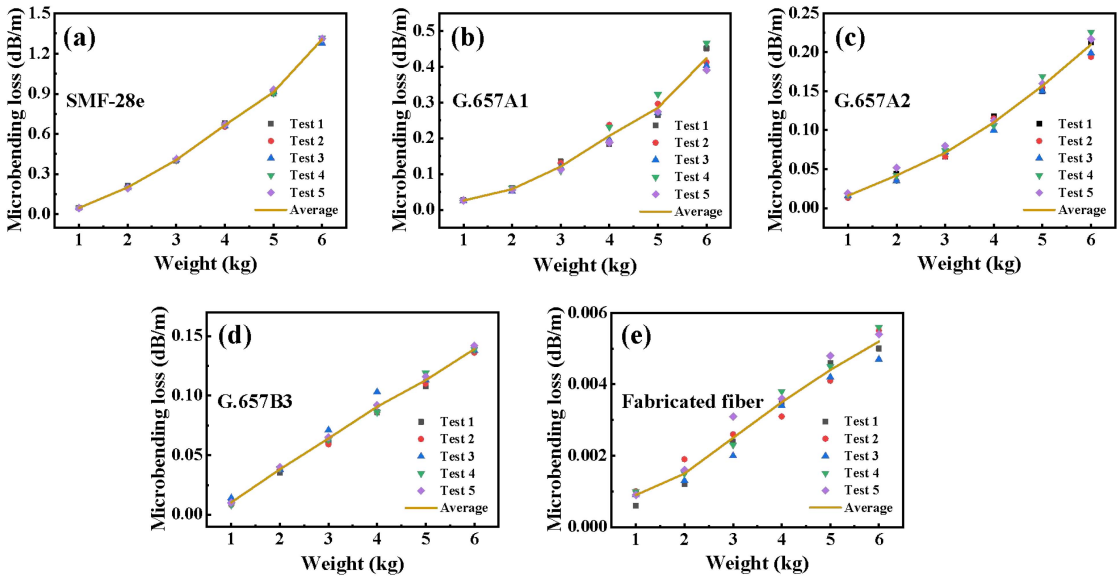

Fig. 11. Experimental results of (a) SMF-28e, (b) G.657A1, (c) G.657A2, (d) G.657B3, (e) fabricated fiber.

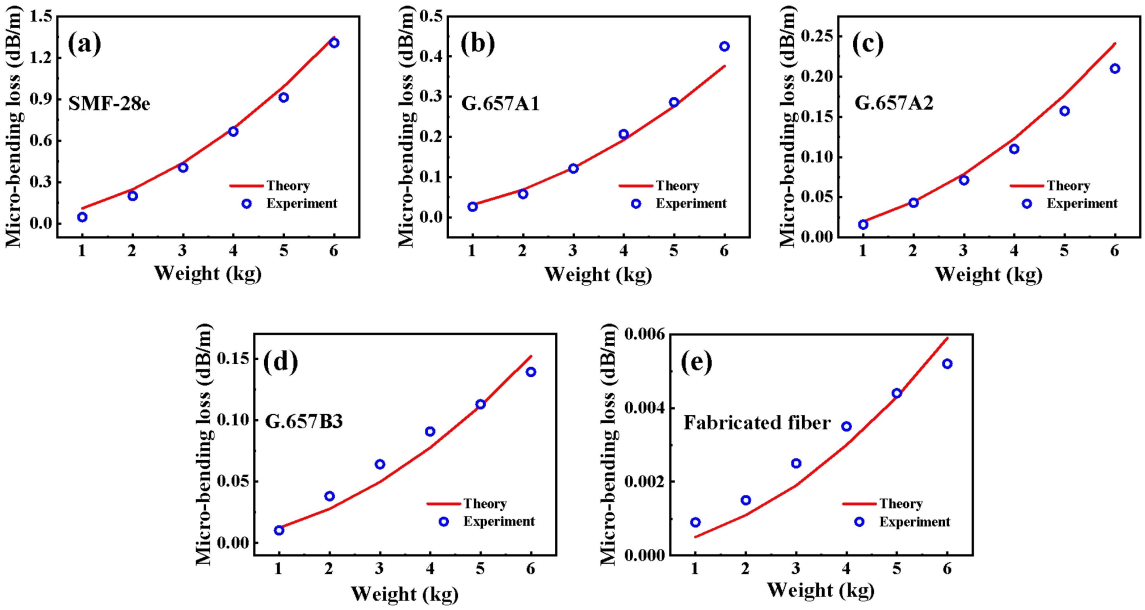

Fig. 12. Comparison between the theoretical and experimental results of (a) SMF-28e, (b) G.657A1, (c) G.657A2, (d) G.657B3, and (e) fabricated fiber.

fiber and the fabricated fiber increase with the weight. The microbending loss of the fabricated fiber is lower at the same weight, which is mainly due to the larger core refractive index of the fabricated fiber at the expense of the mode field diameter and the transmission loss [4]. From the inset of Fig. 9, both the designed fiber and the fabricated fiber effectively confine the light within the core at 6 kg weight at 1550 nm. The core energy ratio of the fabricated fiber is 95.77%, which is slightly higher than the designed fiber's 95.03%. The simulation results indicate that the fabricated fiber exhibits a stronger light confinement capability.

B. Measurement and Discussion of the Microbending Loss

The schematic diagram of the microbending loss measurement system is presented in Fig. 10(a). The optical signal with a wavelength of 1550 nm from a light source (MCSWLS-1550, MC Fiber Optics) is coupled into the optical fiber with a length of 3 m. The microbending deformation of the optical fiber will produce by the microbending-inducing equipment. Finally, the power at the output of the optical fiber is detected by an optical power meter (PM400, Thorlabs). In the measurement, an optical fiber with a spacing of 30 mm and a length of 150 mm is placed parallel to the middle of the base plate. Then, the wire mesh and the top plate with a mass of 1 kg are placed sequentially on top. It is worth mentioning that the base plate and the top plate are made of float glass with a flat and smooth surface so that the load is only borne by the optical fiber. Subsequently, six 1 kg weights are gradually employed to provide the additional load required to induce additional microbending loss. To further improve the reliability and repeatability of the measurement, the positions and order of the six weights are determined, as described in Fig. 10(a). It is necessary that the data should be recorded after waiting for approximately 60 s until the power stabilizes. Fig. 10(b) gives a photograph of the experimental setup for the microbending loss measurement system.

The measured microbending loss of SMF-28e, G.657A1, G.657A2, G.657B3, and the fabricated fiber as a function of the weight at 1550 nm are indicated in Fig. 11. It is evident that the microbending losses of the five optical fibers all increase with the weight. The greater the weight, the greater the degree of the fiber microbending, which results in more light energy leaking from the core into the cladding and external environment. The microbending losses of the five optical fibers at 6 kg weight are 1.306 dB/m, 0.4252 dB/m, 0.2096 dB/m, 0.1392 dB/m, and 0.0052 dB/m, respectively. The microbending loss of the fabricated fiber is reduced by two orders and one order of magnitude than that of SMF-28e and G.657B3, respectively. Compared with the other four fibers, the fabricated fiber exhibits a remarkable improvement in microbending insensitivity. This is mainly because the trenches in the fabricated fiber structure effectively confine the light within the core, greatly reducing the leakage of light energy. The microbending losses of the five fibers were measured once daily for five consecutive days. The standard deviations of the microbending loss measurements are small, with values of 0.0168 dB/m, 0.0324 dB/m, 0.0133 dB/m, 0.0024 dB/m, and 0.0008 dB/m for SMF-28e, G.657A1, G.657A2, G.657B3, and the fabricated fiber at 6 kg weight, respectively. The experimental results demonstrate that the microbending loss measurement system has good reliability and repeatability.

Meanwhile, the cutoff wavelengths and the MFDs of the five fibers were also measured using a comprehensive parameter analyzer (PK2400, Photon Kinetics). The cutoff wavelengths of SMF-28e, G.657A1, G.657A2, G.657B3, and the fabricated fiber were determined to be 1260 nm, 1302 nm, 1316 nm, 1331 nm, and 1407 nm, respectively. The MFDs at 1550 nm of the five fibers were measured to be 10.4 μm, 9.3 μm, 9.1 μm, 8.8 μm,

and 6.8 μm, respectively. Reduction in the MFD can contribute to decreasing the microbending loss of the fiber [31].

Further, the theoretical and experimental microbending losses of SMF-28e, G.657A1, G.657A2, G.657B3, and the fabricated fiber are presented in Fig. 12. It should be noted that the experimental microbending losses of each fiber are the average values of the microbending losses obtained by measuring once daily for five consecutive days. By a suitable choice of the parameter p in (5), a reasonable fit to the experimental data can be obtained using the least squares method [32]. The parameters p acquired are 0.8149, 0.7836, 0.7919, 0.7911, and 0.7732 for the five optical fibers, respectively. The correlation between the theoretical and experimental results of the five optical fibers is good, with correlation coefficients of 0.9991, 0.9982, 0.9996, 0.9830, and 0.9876, respectively. The theoretical results show excellent agreement with the experimental results, thus proving the validity of the theory.

V. Conclusion

In this study, a trench-assisted optical fiber with two trenches beside the core was investigated. The deformation distribution of the fiber axis caused by the wire mesh was obtained by the mechanical-optical model, which is consistent with a Gaussian curve. The formula for the microbending loss in the case of Gaussian deformation was derived. The optimum structure of the trench-assisted optical fiber was determined through a microbending loss simulation. The designed fiber can concentrate most of the energy in the core region under microbending, with a core energy ratio of 95.03%. However, the core energy ratios of SMF-28e, G.657A1, G.657A2, and G.657B3 were 83.33%, 84.59%, 86.03%, and 88.46%, respectively. The designed fiber was fabricated based on the MCVD technique and measured using the modified plate method. The microbending loss of the fabricated fiber was 0.0052 dB/m at 6 kg weight at 1550 nm, while the same attributes for SMF-28e, G.657A1, G.657A2, and G.657B3 were 1.306 dB/m, 0.4252 dB/m, 0.2096 dB/m and 0.1392 dB/m, respectively. Our proposed trench-assisted optical fiber has the feasibility to be applied in deep-ocean exploration for improving communication efficiency.

References

[1] Y. Meng et al., "Dynamics calculation of complex deep-sea cable system based on hybrid optimization algorithm," *Ocean. Eng.*, vol. 200, Feb. 2020, Art. no. 107041.

[2] L. L. Whitcomb et al., "Navigation and control of the nereus hybrid underwater vehicle for global ocean science to 10,903 m depth: Preliminary results," in *Proc. IEEE Int. Conf. Robot. Automat.*, 2010, pp. 594–600.

[3] H. Nakajoh, T. Murashima, and F. Sugimoto, "Development of full depth fiber optic cable ROV (UROV11K) system," in *Proc. OCEANS MTS/IEEE Charleston*, 2018, pp. 1–8.

[4] S. Cao et al., "Design and experimental verification of a novel optical fiber for the full ocean depth communication," *Opt. Commun.*, vol. 478, Aug. 2021, Art. no. 126398.

[5] P. Wang et al., *Mid-Infrared Fluoride and Chalcogenide Glasses and Fibers*. Berlin, Germany: Springer, 2022.

[6] R. Olshansky, "Distortion losses in cabled optical fibers," *Appl. Opt.*, vol. 14, no. 1, pp. 20–21, Jan. 1975.

[7] K. Petermann, "Fundamental mode microbending loss in graded-index and W fibres," *Opt. Quantum Electron.*, vol. 9, pp. 167–175, Sep. 1977.

[8] D. Marcuse, "Microdeformation losses of single-mode fibers," *Appl. Opt.*, vol. 23, no. 7, pp. 1082–1091, Apr. 1984.

[9] Z. Várallyay, T. Mihálffy, and K. Mukasa, "Comparison of different deformation functions modeling micro-bending loss of optical fibers on sandpaper test," in *Proc. Opt. Fiber Commun. Conf. Exhib.*, 2022, pp. 1–3.

[10] P. Sillard, S. Richard, L. A. de Montmorillon, and M. Bigot-Astruc, "Micro-bend losses of trench-assisted single-mode fibers," in *Proc. IEEE 36th Eur. Conf. Exhib. Opt. Commun.*, 2010, pp. 1–3.

[11] Y. Tsuchida, K. Mukasa, and R. Sugizaki, "Analyzing a new mechanism of air holes to suppress micro-bending loss," in *Proc. Nat. Fiber Opt. Engineers Conf.*, 2012, pp. 1–3.

[12] Y. Tsuchida, K. Mukasa, and T. Yagi, "Comparison of microbending loss characteristics between LMA holey fibers and conventional LMA fibers," in *Proc. Opt. Fiber Commun. Conf.*, 2010, pp. 1–3.

[13] B. Overton, X. Meersseman, and F. Gooijer, "Microbending-resistant fiber," in *Proc. Int. Wire Cable Symp.*, 2008, pp. 279–282.

[14] P. Sillard et al., "Micro-bend-resistant low-differential-mode-group-delay few-mode fibers," *J. Lightw. Technol.*, vol. 35, no. 4, pp. 734–740, Feb. 2017.

[15] P. R. Watekar, S. Ju, and W. T. Han, "Design and development of a trenched optical fiber with ultra-low bending loss," *Opt. Exp.*, vol. 17, no. 12, pp. 10350–10363, Jun. 2009.

[16] Y. Lian et al., "Ultralow bending-loss trench-assisted single-mode optical fibers," *Photon. Technol. Lett.*, vol. 29, no. 3, pp. 346–349, Feb. 2017.

[17] P. R. Watekar, S. Ju, Y. S. Yoon, Y. S. Lee, and W. T. Han, "Design of a trenched bend insensitive single mode optical fiber using spot size definitions," *Opt. Exp.*, vol. 16, no. 18, pp. 13545–13551, Aug. 2008.

[18] M. Bigot-Astruc, L. Provost, G. Krabshuis, P. Dhenry, and P. Sillard, "125 μm glass diameter single-mode fiber with A_{eff} of 155 μm^2," in *Proc. Opt. Fiber Commun. Conf. Expo. Nat. Fiber Opt. Eng. Conf.*, 2011, pp. 1–3.

[19] L. Wang et al., "Superposition-assisted 125-μm cladding multi-core fibers with ultra-low inter-core crosstalk and high relative core multiplicity factor," *Opt. Fiber. Technol.*, vol. 67, Oct. 2021, Art. no. 102721.

[20] A. Rostami and S. Makouei, "Single-mode fiber design proposal using evolutionary technique with ultra low bending-loss appropriate in FTTH application," *Optik*, vol. 123, no. 8, pp. 735–738, Apr. 2012.

[21] X. Jin and F. P. Payne, "Numerical investigation of microbending loss in optical fibres," *J. Lightw. Technol.*, vol. 34, no. 4, pp. 1247–1253, Feb. 2016.

[22] K. Petermann, "Microbending loss in monomode fibres," *Electron. Lett.*, vol. 4, no. 12, pp. 107–109, Feb. 1976.

[23] X. Q. Wang, X. H. Xie, S. S. Cao, and C. S. Li, "Microbending test method C analysis and optimization," *Modern Trans.*, vol. 42, no. 5, pp. 63–66, Oct. 2016.

[24] IEC, "Optical fibres – Measurement methods – Microbending sensitivity," IEC, London, U.K., IEC/Tech. Rep. 62221, 2012.

[25] A. V. Velamuri, K. Patel, I. Sharma, S. S. Gupta, S. Gaikwad, and P. K. Krishnamurthy, "Investigation of planar and helical bend losses in single-and few-mode optical fibers," *J. Lightw. Technol.*, vol. 37, no. 14, pp. 3544–3556, Jul. 2019.

[26] R. Ahmad, W. Ko, K. S. Feder, and P. S. Westbrook, "Measuring the shape of microbends in optical fibers," *Opt. Lett.*, vol. 45, no. 18, pp. 5189–5192, Sep. 2020.

[27] J. A. Jay, "An overview of macrobending and microbending of optical fibers," White paper of Corning, 2010. [Online]. Available: https://www.corning.com/media/worldwide/coc/documents/Fiber/white-paper/WP1212.pdf

[28] N. Wang, Y. Liu, W. Li, X. Huo, Y. Liu, and L. Zhang, "Design of a trench-assisted optical fiber for generating Bessel beams with different shapes," *IEEE Photon. J.*, vol. 14, no. 4, Aug. 2022, Art. no. 7145805.

[29] L. P. Zhu, "Research of OPLC on temperature field distribution and optical fiber transmission loss," M.S. thesis, Dept. Elect. Commun. Eng., Harbin Univ. Sci. Technol., Harbin, China, 2014.

[30] K. Worhoff, P. V. Lambeck, and A. Driessen, "Design, tolerance analysis, and fabrication of silicon oxynitride based planar optical waveguides for communication devices," *J. Lightw. Technol.*, vol. 17, no. 8, pp. 1401–1407, Aug. 1999.

[31] Y. B. Liao and M. Li, "Losses in the fiber optic system induced by external factors," in *Fiber Optics*, 1st ed., Beijing, China: Univ. Tsinghua Press, 2000, pp. 93–111.

[32] S. Hornung, N. J. Doran, and R. Allen, "Monomode fibre microbending loss measurements and their interpretation," *Opt. Quantum Electron.*, vol. 14, pp. 359–362, Jul. 1982.